Revision 1
Thallium-rich rust scales in drinkable water distribution systems: a case study from northern Tuscany, Italy

Cristian Biagioni [a,*], Massimo D'Orazio [a], Giovanni O. Lepore [b], Francesco D'Acapito[b], Simone Vezzoni[a]

[a] *Dipartimento di Scienze della Terra, Università di Pisa, Via S. Maria 53, 56126, Pisa, Italy*
[b] *CNR-IOM-OGG, 71 Avenue des Martyrs, F-38043 Grenoble, France*

Abstract: Following the detection of a severe thallium contamination of the drinkable water from the public distribution system of Valdicastello Carducci-Pietrasanta (northern Tuscany, Italy), and the identification of the source of contamination in the Molini di Sant'Anna spring (average Tl content ≈ 15 μg L^{-1}), the replacement of the contaminated water with a virtually Tl-free one (Tl < 0.10 μg L^{-1}) caused an increase in Tl concentration in the drinkable water. This suggested that the pipeline interior had become a secondary source of Tl contamination, promoting its mineralogical and geochemical study. Rust scales samples taken from several pipeline segments, as well as leaching products obtained from these samples, were investigated through scanning electron microscopy, X-ray fluorescence chemical analyses, inductively coupled plasma – mass spectrometry, X-ray diffraction, and X-ray absorption spectroscopy. Thallium-rich rust scales (up to 5.3 wt% Tl) have been found only in pipeline samples taken downstream the water treatment plant, whereas the sample taken upstream contains much less Tl (~ 90 μg g^{-1}). The Tl-rich nature of such scales is related to the occurrence of nano- and micro-spherules of Tl_2O_3 and less abundant nanocrystalline μm-sized encrustations of TlCl. Leaching experiments on Tl-rich rust scales indicate that a fraction of the available Tl is easily dissolved in tap water; X-ray absorption spectroscopy suggests that monovalent thallium occurs in water equilibrated with the rust scales, probably related to the dissolution of TlCl encrustations. Therefore, Tl dissolved as Tl^+ only in the water from the Molini di Sant'Anna spring was partially removed through oxidative precipitation of Tl_2O_3 and precipitation of TlCl. This highlights the critical role played by the addition of chlorine-based oxidants in water treatment plants that could favour the deposition of Tl-rich coatings within the pipelines, giving rise to unexpected secondary sources of contamination.

Graphical abstract

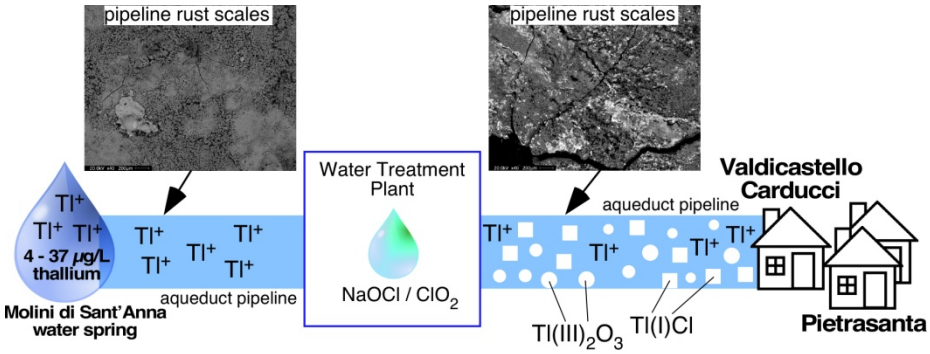

Keywords: thallium; drinkable water; emerging pollution; water treatment; X-ray Absorption Spectrometry

1. Introduction

Thallium (Tl) is a highly toxic element for the humans and many other living organism (e.g., Ralph and Twiss, 2002; Peter and Viraraghavan, 2005; Xiao et al., 2007), and it is classified as one of the 13 priority metal pollutants (Keith and Telliard, 1979). Nonetheless, its admissible concentration in drinkable water is not regulated in most countries, two notable exceptions being the U.S.A., where the Environmental Protection Agency set a maximum contaminant level (MCL) in drinkable water of 2.0 μg L^{-1} (with a maximum contaminant level goal, MCLG, of 0.5 μg L^{-1}), and China, that set such a maximum concentration level of Tl at 0.1 μg L^{-1} (China MH, 2006). The occurrence of Tl in drinkable water at concentrations of concern should not be considered as exceptional or extremely rare because the average concentration of this element in the Upper Continental Crust of the Earth is about 0.75 mg kg^{-1} (Wedepohl, 1995), comparable to the concentration of other metals and metalloids such as As, Be, Cd, Ge, Hg, Mo, Sb, Sn, and U. Moreover, Tl is highly soluble in water and its removal from the aqueous system occurs only in peculiar physico-chemical conditions. Water contamination by Tl may occur due to both natural and anthropogenic causes. Areas hosting significant amounts of Tl-bearing sulfide ores are potential sites for Tl contamination of superficial and/or groundwaters. Thus, drinkable waters springing within these areas should be more carefully monitored for the presence of this heavy element.

In September 2014 a severe Tl contamination of drinkable water was discovered by one of the authors of this paper (MD) in the public aqueduct serving the village of Valdicastello Carducci (hereafter Valdicastello, about 1000 inhabitants) and part of the town of Pietrasanta (about 25,000 inhabitants), northern Tuscany, Italy. Analyses of urine and hair of people resident in the contaminated area revealed a significant accumulation of Tl in these biological matrices (Campanella et al., 2016) compared to the reference values of Italian population. The source of the water contamination was promptly identified in a spring located within a mineralized area formerly site of mining activity for baryte-pyrite-iron oxides-(Pb-Zn-Ag). As the water contamination persisted following the replacement of the contaminated spring with a Tl-free spring, it was realized that Tl had accumulated in high amounts, and in unknown form, in the rust scales that commonly line the internal surfaces of old steel pipelines, thus forming a secondary source of Tl contamination.

Even if Tl contamination has been reported from other localities worldwide (e.g., http://www.ewg.org/tap-water/chemical-contaminants/Thallium-total/1085/), the high Tl contents determined in drinkable water (up to about 80 μg L^{-1}) and the detection of the Tl enrichment of rust scales lining the pipelines of the Valdicastello-Pietrasanta aqueduct represent a *unicum* world-wide.

Moreover, the identification of the Tl solid phases gives some insights on the thallium speciation in rust scales of aqueduct pipelines and underlines the potential role played by water treatment in favoring the accumulation of thallium, giving rise to unexpected secondary sources of contamination.

This paper reports the results of the mineralogical and geochemical study of the Tl-rich rust scales lining the Valdicastello-Pietrasanta aqueduct pipeline, discussing the possible causes of this exceptional accumulation of Tl compounds.

2. Thallium contamination of drinkable water at Valdicastello – Pietrasanta

Following the first identification of Tl minerals in the ore deposits of the Apuan Alps (Orlandi et al., 2012), Biagioni et al. (2013) reported the Tl-rich nature (up to 1100 mg kg^{-1}) of pyrite ores from a series of baryte-pyrite-iron oxide orebodies aligned along a ~ 10 km belt in the southern Apuan Alps and mined up to the end of the 1980s. This finding was later detailed by D'Orazio et al. (2017), emphasizing the threats related to the thallium dispersion in the environment following pyrite oxidation. The occurrence of very high concentrations of Tl (commonly > 200 μg L^{-1} and up to 9000 μg L^{-1}; Campanella et al., 2016) in mine waters is particularly striking, indicating the passage of Tl from litosphere to hydrosphere and, potentially, to biosphere. In this respect, the occurrence of pyrite-rich ore bodies in this area poses a serious threat to the vulnerability of superficial and groundwaters.

At the beginning of September 2014, a series of water samples taken from several public fountains of Valdicastello were analysed by one of the authors (MD). It was found that the water tapped from these fountains contained between about 2 and 10 μg L^{-1} of Tl, with a progressive decrease of Tl concentration downstream. After the report to the public authorities, on October 3, 2014 the Major of Pietrasanta disposed a "Not to drink" order for the inhabitants of Valdicastello. The source of the Tl contamination was soon identified in the Molini di Sant'Anna water spring. This spring fed, very likely since 1951, the aqueduct of Valdicastello and part of the aqueduct of Pietrasanta. This is a karst water spring emerging at the base of a large (0.16 km^2) paleo-landslide, close to the contact between Paleozoic quartz-muscovite-chlorite schist and Upper Triassic metadolostone, about 1400 m northeast of Valdicastello, at an altitude of 318 m above sea level (Fig. 1). This locality lies in between the abandoned mines of Pollone and Monte Arsiccio in an area characterized by the widespread occurrence of baryte, pyrite, magnetite, hematite, and iron hydroxide mineralizations. Selected physico-chemical features of this spring are given in Table 1. During the period October 2014 – April 2016, the Tl content of the water flowing from this spring

was always above the maximum level of 2.0 μg L^{-1} set by the Italian laws for underground waters. Ion exchange chromatography coupled with ICP-MS revealed that only Tl(I) occurs in the water spring (M. Onor, personal communication).

Immediately after the detection of its contamination, the spring was excluded from the drinking water distribution system and its water was let to flow into the Baccatoio stream. The water from the Molini di Sant'Anna spring was replaced by the water flowing from another spring, named Moresco Galleria, located within the Valdicastello village and characterized by low Tl contents (< 0.10 μg L^{-1}). Surprisingly, as soon as the water from the Moresco Galleria spring flowed inside the pipeline, the Tl concentrations in the public fountains increased (up to about 80 μg L^{-1}). The causes of this increase of Tl concentration were tentatively ascribed by local authorities to the removal of Tl-bearing "sediments" lining the internal surfaces of the aqueduct pipeline. The mechanical removal of the "sediments" would have been caused by the flow of the Moresco Galleria spring waters, directed upstream from the spring to the water treatment plant, in the opposite sense with respect to the former downstream flow from the Molini di Sant'Anna spring (Fig. 1). Even if this explanation was not entirely convincing, it demonstrated that the pipeline interior had accumulated Tl becoming a secondary source of Tl contamination. Consequently, about 6.5 km of the old steel pipelines proximal to the water treatment plant were substituted with new PVC pipelines, whereas distal pipelines were flushed through ice pigging + CO_2 by GAIA S.p.A., the public company responsible for drinkable water supply in this area.

3. Samples and analytical methods

3.1. Samples and their preparation

Four segments of the aqueduct pipeline serving the village of Valdicastello and the town of Pietrasanta were made available to the authors by GAIA S.p.A. in November 2014, following their removal from the water distribution system. The pipeline segments are numbered from #1 to #4 in order of increasing distance from the Molini di Sant'Anna water spring (Fig. 1). In particular, pipeline samples P#1 and P#2 were taken immediately before (inlet) and immediately after (outlet) the water treatment plant, respectively. Pipeline samples P#3 and P#4 were taken downstream the water treatment plant about 350 and 1600 m, respectively, from the plant itself. Pipeline samples are from 16 to 50 cm in length and have an internal diameter of 110 mm (samples P#2, P#3, P#4) or 135 mm (sample P#1) and thickness of 5-7 mm. About 20 g of rust scales were taken from each pipeline sample and finely powdered in agate mortar and pestle.

A series of basic leaching experiments was performed to evaluate i) how much Tl contained in the scales could be dissolved into water and ii) which is the form of soluble Tl. About 25 to 150 mg of powdered samples were dispersed in variable volumes (10 to 50 ml) of tap water (Tl < 0.05 µg L^{-1}, *p*H = 7.6). The slurries were sonicated for 1 min and left in quiet for 12-24 hours at room temperature. In most experiments the supernatant was filtered at 0.20 µm or 0.45 µm with Teflon membrane filters and stored in plastic vials.

About 1 g of powdered sample P#2 (the sample containing the highest Tl concentration) was dispersed in 20 mL of ultrapure water, sonicated for 1 min, and left in quiet for 24 hours at room temperature. The Tl content in the final solution (*p*H = 7.4) was 110 mg L^{-1}. About 9 mL of supernatant were filtered at 0.20 µm and very slowly evaporated to dryness in a plastic container at room temperature, finally obtaining tiny (up to 500 µm) colorless crystals. Two additional 5 mL aliquots of supernatant, filtered at 0.20 µm, were used in the oxidation experiments with NaOCl and ClO_2, two reagents commonly used in drinking water treatment plants (WHO, 2008).

In order to fully-characterize the rust scales occurring in the pipeline samples and the leaching products, chemical as well as crystallographic data were collected through a multi-technique approach.

3.2. X-ray fluorescence and ICP-MS data collection

Back-scattered and secondary electron images, as well as qualitative chemical data, were obtained using a Philips XL30 SEM equipped with an EDAX DX4 EDS-XRF spectrometer.

The chemical composition of the pristine metal of the pipes was obtained by XRF using a Hand-Held XRF-EDS spectrometer (Niton XL3t 980 Goldd+, beam spot diameter 3 mm, ~7 mm^2) on a cleaned and polished surface of sample P#3. The same spectrometer was used to qualitatively investigate the composition of the internal scaly surface of the pipes of samples P#1–P#4.

The concentration of Tl (and several additional elements) of the bulk scale material was determined by ICP-MS for samples P#1, P#2, and P#3. About 50 mg of powdered samples were dissolved with a mixture of superpure HF + HNO_3 in perfluoralkoxy (PFA) vials on a hot plate. After appropriate dilution with ultrapure water (Millipore Milli-Q, > 18.2 MOhm cm), the sample solutions were analyzed for Tl, Mn, Al, and Zn with a Perkin-Elmer NexION 300x spectrometer. A solution containing 20 ng mL^{-1} of Rh and Bi (internal standards) was mixed on-line with the sample solutions just before reaching the nebulizer. The instrument was calibrated with synthetic solutions made by diluting and mixing 10 µg mL^{-1} single element stock solutions (Inorganic Ventures).

An aliquot of supernatant water of each leaching experiment was diluted with ultrapure water and analyzed by ICP-MS. The detection limits for the determined elements, calculated as three times the standard deviation of the concentrations of blank solutions plus the average blank concentration (N=32) are: Tl = 0.05 μg L^{-1}, Al = 15 μg L^{-1}, Mn = 0.2 μg L^{-1}, Zn = 10 μg L^{-1}. These concentrations are several orders of magnitude lower than those measured in the studied samples. At the concentrations found in the samples, the analytical precision of the ICP-MS measurements for Tl, Al, Mn, and Zn are typically better than 5% RSD.

All these investigations were carried out at the Pisa University's Dipartimento di Scienze della Terra.

3.3. X-ray diffraction study

The nature of the thallium-bearing solid phases was determined by X-ray diffraction (XRD) using both a 114.6 mm Gandolfi camera and a Bruker D2 Phaser diffractometer (30 kV, 10 mA) operating in Bragg-Brentano geometry (θ-θ scan mode) and equipped with a one-dimensional Lynxeye detector. Nickel-filtered Cu *K*α radiation was used in both cases. The uncertainty on the accuracy of the measurement of the angular position of the X-ray diffraction effects is less than 0.02° in 2θ.

X-ray diffraction studies were performed at the Pisa University's Dipartimento di Scienze della Terra.

3.4. X-ray Absorption Spectroscopy

In order to investigate the incorporation site and speciation of Tl within the rust scales, X-ray Absorption Spectroscopy (XAS) measurements at the Tl-L_3 edge (12658 eV) were performed at the LISA beamline (BM-08, d'Acapito et al., 2016) at the European Synchrotron Radiation Facility (ESRF, Grenoble – France). The main beamline optical features include a fixed exit dynamically focusing monochromator with a pair of Si [311] crystals, and a pair of Pd coated mirrors for harmonics rejection ($E_{cutoff} \approx 18$ keV). Spectra were acquired in the energy range 12458-13206 eV. The energy sampling interval in the near edge region (12638–12688 eV) was 0.5 eV. In order to reduce the thermal damping of the signal and to prevent possible beam-induced redox reactions, all samples were measured at 80 K.

Samples P#2 and P#3 were powdered, mixed with cellulose and pressed in pellets using an amount of material such as to keep the total absorption (μ) ≤1.5 above the edge. Moreover, the

206 water leachate (sample leach_P#2-*aq.*), the residual solid fraction (sample res_P#2), and the salts
207 obtained evaporating the leachate (sample leach_P#2-*ev*) were measured.
208 The spectra of the model compounds Tl_2O_3 and Tl_2SO_4 were collected in transmission mode.
209 All other samples were measured in fluorescence mode by means of a 12-elements solid state (high
210 purity Germanium) detector.
211 All samples contained a considerable amount of Fe and in order to prevent the detector pile-up
212 (caused by the Fe fluorescence yield) a 250 μm Al filter was placed in front of the detector in
213 fluorescence measurements of rust scales (samples P#2, res_P#2, P#3).
214 A Se (Se *K*-edge= 12658 eV) reference was placed before a third ionization chamber, allowing
215 to acquire a spectrum simultaneously with each measurement on the samples and thus accurately
216 calibrate the energy.
217 A minimum of four spectra was collected for each sample, with the exception of Tl_2SO_4 and
218 Tl_2O_3 standards (one and two spectra, respectively) and the two leachate (one spectrum each). The
219 software ATHENA (Ravel and Newville, 2005) was used to calibrate energy (eV) and to average
220 multiple spectra.
221
222 **4. Results**
223
224 *4.1. Structure, mineralogy, and geochemistry of Tl-rich rust scales*
225 The internal surfaces of the pipes show a heterogeneous nature with centimetre-sized patchy
226 areas coloured from light orange to black. The surface is rough due to the occurrence of tubercles
227 up to 2 cm wide and 1 cm high. The rust scales have a thickness of about 0.5-1 mm and show a
228 sharp contact with the metal of the pipe. Under the optical stereomicroscope, many bright black
229 micro-spherules scattered onto or embedded in the rust scales can be observed in all samples (Fig.
230 2). These spherules are attracted by a magnet and have diameters variable from few tens of
231 nanometers up to a maximum of 200 μm. Detrital crystals of quartz, muscovite, and baryte, up to
232 100-200 μm in size, are also commonly observed.
233 Several scales taken from the four samples have been examined by scanning electron
234 microscopy. Back-scattered electron (BSE) images reveal that the scales of the three pipeline
235 samples taken downstream the water treatment plant (i.e., P#2, P#3, and P#4) are characterized by a
236 strong chemical heterogeneity, revealed by the occurrence of high reflective spots peppering their
237 surface or embedded in the first few tens of μm from the surface of the rust scales (Fig. 2). On the
238 contrary, sample P#1, taken at the inlet of the water treatment plant (Fig. 1), displays a
239 homogeneous reflectivity (Fig. 2).

The dominant material forming the rust scales (grey to dark-grey in BSE images) is composed by Fe, O, and minor Mn, as determined by XRF-EDS analyses. It appears as crusts and nano- to micro-spherules. The high reflective spots occurring only in samples P#2-4 are formed by abundant nano- and micro-spherules and rarer nanocrystalline µm-sized crusts (Fig. 3). The spherules, up to 20 µm in size, show smooth external surfaces and an "onion-shell" internal structure. They occur both on the surface of the scales or embedded in them (Fig. 3a, b, c). Qualitative XRF-EDS analyses show that these particles are composed by Tl and O only. The nanocrystalline encrustations are made of less than about 2 µm-sized rounded and hollow crystals occurring just on the surface of the rust scales (Fig. 3d, e, f). Chemically, they are formed by Tl and Cl.

A very small black fragment characterized by high abundance of Tl-O micro-spherules, a magnetic Fe-(Mn)-O spherule, and a fragment of orange-brown rust were taken from sample P#3 for XRD analysis. The XRD patterns of the magnetic spherule and of the rust material indicate that they are made of magnetite + wüstite and poorly-crystalline Fe-hydroxides, respectively. The XRD pattern of the Tl-O spherules is presented in Fig. 4, along with the calculated XRD pattern of avicennite (Tl_2O_3), based on the crystallographic data given by Otto et al. (1993). On the basis of the observed reflections, the refined unit-cell parameter, calculated using the software UnitCell (Holland and Redfern, 1997), is a = 10.515(1) Å, V = 1162.5(4) Å^3.The close match of the two XRD patterns allows us to identify the (Tl-O) nano- and micro-spherules occurring inside the pipeline of the Valdicastello-Pietrasanta aqueduct as Tl_2O_3. Owing to the small size of the Tl-Cl crusts, it was not possible to collect any XRD pattern.

The rust scales were qualitatively analyzed *in situ* through HHXRF, in order to check the Tl abundance in the four pipeline samples. In agreement with SEM observations, the most interesting results are those obtained on samples P#1 and P#2 (Fig. 5), showing striking differences in the Tl contents. Indeed, sample P#1, taken before the water treatment plant, shows only very low amounts of Tl, whereas sample P#2, taken after the treatment plant, contains huge amounts of this element. X-ray spectra similar to that of sample P#2 characterize also samples P#3 and P#4. For the sake of completeness, the composition of the pristine metal of the pipelines was also determined through HHXRF. Five replicate analyses gave the following results (in wt%): Fe = 98.78 ± 0.01 (2 × SD), Mn = 0.705 ± 0.009, Cu = 0.248 ± 0.001, Ni = 0.110 ± 0.006.

The bulk concentrations of the internal rust scales, measured through ICP-MS, are reported in Table 2. In addition to Fe (not determined) the rust scales contain about 0.3-0.4 wt% Mn and 0.12-0.16 wt% Al. The concentrations of Tl are highly variable, in agreement with previous observations, and range from the relatively low value of sample P#1, taken immediately before the water

treatment plant, to the extremely high value (5.3 wt%) of sample P#2, taken immediately after the water treatment plant. Sample P#1 is also characterized by high contents of Zn.

4.2. Leaching and oxidation experiments

The results of the leaching experiments are shown in Table 3. They indicate that about 23% (± 3%) of the Tl available in the rust scales of sample P#3 (1.52 wt% Tl) is easily dissolved in tap water. Because Tl_2O_3 is nearly insoluble in water ($10^{-5.8}$ m at *p*H 7 and $10^{-11.7}$ m at *p*H 9 and Eh 0.55 V; Xiong, 2009), these data confirm the occurrence of other Tl species within the pipeline.

The evaporation of the supernatant lead to the precipitation of tiny colorless crystals, showing different morphologies. SEM study showed that gypsum and TlCl are the main phases crystallizing from this medium. Thallium(I) chloride occurs as cubic crystals, up to 200 μm in size (Fig. 6); their identification was further confirmed through XRD. Thallium(I) chloride is a moderately soluble Tl salt (3.3 g L^{-1} at 20 °C; Hammond, 2004-2005).

The two additional 5 mL aliquots of supernatant were treated with 0.1 mL of a ~1.2 wt% NaOCl solution (*p*H = 11.7) and 1 mL of a ~2 wt% ClO_2 solution (*p*H = 8.0), respectively. In both cases, after about one hour from the addition of the oxidant, a dark brown solid precipitated from the solution (Fig. 7). The precipitates, examined through XRD, are represented, in both experiments, by Tl_2O_3.

Even if these experiments do not reproduce the actual physico-chemical conditions occurring within the water distribution system, they prove that Tl-rich rust scales are potentially able to release high Tl concentrations in water. Moreover, it has been proved that the addition of chlorine-based oxidants is able to precipitate Tl_2O_3.

4.3. X-ray Absorption Spectroscopy (XAS) results

4.3.1. X-ray Absorption Near-Edge Structure (XANES)

The XANES absorption spectra (normalised and first derivative) of measured samples and reference compounds are reported in Figs. 8a and 8b. Results on standards agree with literature data (e.g., Scheckel et al., 2004; Agarwal and Vishnoi, 2005; Dutrizac et al., 2005; Peacock and Moon, 2012), as monovalent compounds show a single absorption peak while Tl_2O_3 shows a weak peak, followed by a shoulder on rising absorption, culminating in a marked peak. The XANES region of samples P#2, res_P#2, and P#3 spectra closely resemble that of Tl_2O_3 (absorption edge at ~12669 eV), despite, especially in the case of P#3 sample, the presence of a shoulder situated in correspondence of the position of Tl(I) edge, clearly observable in the normalized as well as in the

first derivative absorption spectra. This latter observation suggests the presence of two different signals arising from both Tl(I) and Tl(III).

This idea is further confirmed by the analysis of the leachate sample (leach_P#2-*aq*. and leach_P#2-*ev*) whose spectrum shows indeed the presence of only Tl(I) (Fig. 8a, b), in agreement with the very low solubility of Tl_2O_3 and with the leaching experiments described above.

4.3.2. Extended X-ray Absorption Fine Structure (EXAFS)

Standard procedures (Lee et al., 1981) were followed to extract the structural EXAFS signal ($k \bullet \chi(k)$): pre-edge background removal, spline modelling of bare atomic background, edge step normalization using a far above the edge region, and energy calibration. Model atomic clusters centred on the absorber atom were obtained by ATOMS (Ravel, 2001) using the crystallographic structure reported in the literature by Otto et al. (1993) for Tl_2O_3. Theoretical amplitude and phase functions were generated using the FEFF8 code (Ankudinov et al., 1998).

The EXAFS spectra of P#1, P#2, res_P#2 and P#3 were fitted through the ARTEMIS software (Ravel and Newville, 2005) in the Fourier-Transform (FT) space. For P#2, res_P#2 and P#3, k range was 2-10.15 $Å^{-1}$ and weight 2; the FT range was 1.3-4 Å. Hanning windows were used. Amplitude factors for first-shell were calculated on the basis of bond-valence method (BVM), relating coordination number (CN) to bond distance (R) (Brown, 2002) with the exception of P#3 (see below).

Tl L_3-edge EXAFS and Fourier transform of measured samples are shown in Figs. 8c and 8d, respectively. The corresponding multiparameter fits are also reported in the same figure; fit results are shown in Table 4.

The features of the samples from rust scales are, as in the XANES region, congruous with those of pure Tl_2O_3; nonetheless it is possible to note how the amplitude of oscillations is much smaller compared to that of Tl_2O_3. This can be seen as a hint of a disordered Tl site; it is also worth noting that the sample showing the most marked decrease in amplitude is P#3 that also shows strong indications of the presence of a monovalent Tl phase in the XANES region. The corresponding Fourier transform moduli present a first shell-peak centred at about 1.6 Å followed by two smaller peaks at about 2.9 and 3.3 Å, in agreement with those shown by Tl_2O_3.

The quantitative analysis showed that the first shell is formed by O atoms, while the second shell is attributed to two slightly different Tl–Tl distances. In the case of P#2 and res_P#2, both coordination number and interatomic distances are in fair agreement with those found in Tl_2O_3 while in P#3, despite interatomic distances remain consistent with those of Tl_2O_3, coordination numbers appear much lower than those expected. Together with the large Debye-Waller values, this is a strong indication of a co-presence of multiple phases for Tl, whose signals tend to cancel due to

a destructive interference. This is consistent with the two different local environments suggested by XANES analysis.

XAS data show that Tl in rust scales is present in two different phases. As highlighted by both EXAFS and XANES results, the main one is Tl_2O_3. Nevertheless, the presence of another, more disordered, Tl(I) phase is clearly noticeable.

5. Discussion

5.1. The precipitation of Tl_2O_3 in the pipeline: a possible role of water treatment

The most striking feature of the rust scales within the aqueduct pipeline is represented by the occurrence of detectable amounts of Tl_2O_3, confirmed through X-ray diffraction and X-ray Absorption Spectroscopy. Naturally occurring Tl_2O_3 is known as the mineral avicennite, so far found in less than ten localities world-wide and occurring as brownish-blackish coatings resulting from the alteration of Tl-bearing ores (e.g., Anthony et al., 1990). Its presence in the rust scales was completely unexpected, because in the majority of natural conditions of aqueous systems, the most stable species of thallium is Tl(I). Indeed, in Eh-*p*H diagrams this species is soluble both in strongly acidic and strongly alkaline solutions at intermediate values of Eh.

Insoluble thallium species can be stabilized either under highly oxidizing conditions as $Tl(III)(OH)_3$ or $Tl(III)_2O_3$, or under highly reducing conditions in sulfur-bearing systems as $Tl(I)_2S$ or metallic thallium. Because Tl dissolved in the water of the Molini di Sant'Anna spring is Tl(I) only, the occurrence of Tl_2O_3 in the aqueduct pipelines is consequently related to the oxidation of Tl(I) and its subsequent precipitation. It is worth noting that several methods proposed for the removal of Tl from the aqueous systems involve their oxidative precipitation (e.g., Davies et al., 2016). Indeed, the oxidative precipitation of thallium as Tl(III) hydroxides and oxides is considered an effective process to remove thallium from solutions as both species are insoluble in water. The most common oxidizing agents tested in thallium removal experiments are hydrogen peroxide (H_2O_2), sodium hypochlorite (NaOCl), chlorine dioxide (ClO_2), and potassium permanganate ($KMnO_4$).

Sodium hypochlorite and chlorine dioxide are two of the most widely used reagents in drinkable water treatment plants. These reagents are used as disinfectants and to oxidize excessive amounts of dissolved Fe^{2+} and Mn^{2+} to insoluble $Fe(III)(OH)_3$ and MnO_2, afterwards removed by filtration (WHO, 2008). The water treatment plant of Valdicastello formerly used NaOCl that was replaced in 1996/97 by ClO_2, generated "in situ" through the reaction (1) of sodium chlorite with

hydrochloric acid (F. Di Martino, GAIA S.p.A., personal communication):

$$5\ NaClO_2 + 4\ HCl = 5\ NaCl + 4\ ClO_2 + 2\ H_2O \quad (1)$$

Dissolving NaOCl into water, the species Cl_2, HOCl, and OCl^- could occur when the system approach equilibrium. The ratio Cl_2/HOCl/OCl^- is *p*H-dependant. Above a *p*H value of ~7.5, OCl^- should be the dominant species, whereas between 5 and 7.5 HOCl should prevail over OCl^-. Therefore, in slightly acidic, circumneutral, and alkaline solutions NaOCl should be able to oxidize dissolved Tl^+ to Tl_2O_3 according to reactions (2) or (3):

$$3\ OCl^- + 2\ Tl^+ + 2\ e^- = 3\ Cl^- + Tl_2O_3 \quad (2)$$

$$6\ HOCl + 2\ Tl^+ + 8\ e^- = 6\ Cl^- + Tl_2O_3 + 3\ H_2O \quad (3)$$

Indeed, the reduction potentials at 25°C of OCl^- (4) and HOCl (5) are 0.81 V and 1.482 V, respectively, whereas the oxidation potential of Tl^+ to Tl_2O_3 is -0.02 V (6) (Vanysek, 2004).

$$OCl^- + H_2O + 2\ e^- = Cl^- + 2\ OH^- \quad 0.81\ V \quad (4)$$

$$HOCl + H^+ + 2\ e^- = Cl^- + H_2O \quad 1.482\ V \quad (5)$$

$$2\ Tl^+ + 6\ OH^- = Tl_2O_3 + 3\ H_2O + 4\ e^- \quad -0.02\ V \quad (6)$$

Chlorine dioxide should be able to oxidize dissolved Tl^+ to Tl_2O_3 according to reaction (7) because the reduction potential of ClO_2 to ClO_2^- (8), the most likely reaction for circumneutral waters, is 0.954 V (Vanysek, 2004)

$$4\ ClO_2 + 2\ Tl^+ + 6\ OH^- = Tl_2O_3 + 3\ H_2O + 4\ ClO_2^- \quad (7)$$

$$ClO_{2(aq)} + e^- = ClO_2^- \quad 0.954\ V \quad (8)$$

In addition to these theoretical data, suggesting the oxidation of Tl(I) to Tl(III) through water treatment, the role of this process in the precipitation of Tl_2O_3 is further supported by three main observations:

i) Tl_2O_3 occurs only downstream with respect to the water treatment plant, whereas pipeline sample P#1, taken immediately before of the plant, shows Tl-poor rust scales and is completely devoid of Tl_2O_3 particles;

ii) Tl_2O_3 spherules are characterized by an "onion-shell" texture, suggesting their growth through successive and discrete pulses, probably related to discontinuities in the addition of NaOCl or ClO_2 to water;

iii) basic experiments confirm that Tl(I)-rich solutions treated with NaOCl and ClO_2 could easily and rapidly precipitate Tl_2O_3.

5.2. Tl-rich rust scales: a secondary source of Tl contamination

Thallium(III) oxide is virtually insoluble in water (Xiong, 2009); consequently, the increase in Tl concentration detected as soon as the water from the Moresco Galleria spring flowed inside the pipeline could be related to a mechanical effect removing Tl_2O_3 nano- and micro-particles from rust scales. However, SEM observations coupled with XRF-EDS analyses, leaching experiments, as well as XAS data, firmly support the occurrence of the moderately soluble compound TlCl in the rust scales in addition to the insoluble Tl_2O_3 (Fig. 3f). The precipitation of TlCl in the pipelines is likely due to the occurrence of excess chloride ions following the addition of NaOCl/ClO_2.

Thus, Tl dissolved as Tl^+ only in the water from the Molini di Sant'Anna spring was massively removed from the water through both oxidative precipitation as Tl_2O_3 and precipitation of TlCl, forming Tl-rich rust scales with Tl contents up to 5.3 wt%. It is worth noting that the nature of the Tl-rich rust scales is the result of processes integrated over a period of time of several decades (likely since 1951). Assuming, over the period 1951–2014, that the spring had an average water flow of 40 ± 10 L s^{-1}, with an average Tl content of 15 ± 5 µg L^{-1}, a total amount of Tl variable between 600 and 2000 kg flowed within the pipeline of the Valdicastello aqueduct.

XAS experiments indicate a decrease in the Tl(III):Tl(I) ratio downstream from the water treatment plant. This suggests that the transport of Tl_2O_3 within the pipeline could be related to a mechanical effect, whereas the TlCl dispersion could be controlled by solubility equilibria, favouring the finding of Tl far away from the water treatment plant.

In conclusion, the addition of NaOCl/ClO_2 in the water treatment plant of Valdicastello is likely critical, favouring the deposition of Tl-rich coatings within the pipelines. This process has a two-fold importance: i) it temporarily subtracted a fraction of thallium from the drinkable water, decreasing the bioavailability of this heavy element; and ii) it gave rise to an unexpected source of contamination.

5.3. Could thallium in drinkable water be more common than thought?

Thallium is a relatively rare but widely dispersed element; as reported above, its average abundance in the Earth's continental crust is comparable to that of other well-known toxic elements, e.g., As, Hg, Sb. However, it was often undetected by classical analytical methods having poor sensitivity for Tl; only the advent of inductively coupled plasma – mass spectrometry allowed routinary analyses of this heavy element. The discovery of the Tl anomaly in the southern Apuan Alps exemplifies such a statement. Notwithstanding decades of mining activity and several scientific studies on these orebodies (e.g., Lattanzi et al., 1994), Tl has not been detected up to the first finding of Tl sulfosalts as accessory minerals in one of these small ore deposits (Orlandi et al., 2012).

Thallium-bearing sulfide ore deposits are known from other localities world-wide, e.g., Meggen, North-Rhine Westfalia, Germany (Krebs, 1981), Allchar, Republic of Macedonia (Volkov et al., 2006), Carlin, Nevada, USA (Radtke, 1985), and Lanmuchang, Ghizou Province, China (Zhang et al., 2000). In addition, Tl can substitute for K in several common rock-forming minerals (e.g., micas, alkali feldspars, feldspathoids). Therefore, this element could be relatively abundant in K-rich rocks, thus representing a further potential source for Tl dispersion in environment (e.g., Calderoni et al., 1983). Consequently, the passage of Tl from the lithosphere to the hydrosphere could be a relatively common phenomenon, posing serious concerns about drinkable water quality. Indeed, several occurrences of Tl contamination in treated tap water have been reported (e.g., http://www.ewg.org/tap-water/chemical-contaminants/Thallium-total/1085/); even if most of them are just above the MCL, they could represent health hazards.

It is worth noting that the Tl hazard is not necessarily related to mining sites. Indeed, in addition to anthropogenic sources, natural sources for metal pollution should not be neglected. As an example, during the period October 2010 – February 2012, the drinkable water emerging from the Traverse Mountain Well (Lehi, Utah Co., Utah) was found to contain between 2.5 and 3.0 μg/L of Tl (UDH, 2014). To the authors' knowledge, this is a case of natural Tl contamination of drinkable water. Therefore, the contribution of Nature to pollution should be taken into account when looking for the source of problems involving metal contamination.

6. Conclusions

Thallium is a highly toxic element, potentially representing a hidden geoenviromental health hazard (e.g., Léonard and Gerber, 1996; Xiao et al., 2004), as proved by several occurrences of Tl contamination above the MCL reported from several countries.

The Tl contamination of the drinkable water of Valdicastello-Pietrasanta is, to the writers' knowledge, a *unicum* and the exceptionally high concentration of Tl found in the aqueduct pipelines

has never been found in other occurrences world-wide. Its detection is the result of the interplay between mineralogy and geochemistry, allowing first the finding of the Tl-rich nature of pyrite orebodies (Biagioni et al., 2013; D'Orazio et al., 2017) and then promoting the investigation of the thallium dispersion in the environment. In this way, the contamination of drinkable water was discovered. The identification of Tl-rich rust scales within the pipelines allowed the understanding of the unusual behaviour of thallium, whose concentration in tap water surprisingly increased after the replacement of the contaminated water spring with a Tl-free one.

Such a high Tl content in rust scales lining the old steel pipelines has a two-fold significance. Indeed, the addition of chlorine-based oxidants to drinkable water induced the temporary sequestration of Tl from water, immobilizing it in solid phases. This process contributed to decrease the bioavailable Tl in drinkable water, thus possibly reducing the harmful effects on the population of Valdicastello-Pietrasanta. However, the precipitation of Tl solid phases on the rust scales gave rise to a new and unexpected secondary source of contamination. As stated above, the nature of the Tl-rich rust scales studied in this work is the result of processes integrated over a period of several years, leading to the accumulation of Tl up to concentrations of some wt% within the pipeline downstream and closer to the water treatment plant.

The multitechnique study of the Tl contamination in the Valdicastello-Pietrasanta area highlights the fundamental role played by mineralogy and geochemistry in managing the natural resources, as recently stressed by other studies (e.g., Ludden et al., 2015).

Acknowledgements

This research received support by Ministero dell'Istruzione, dell'Università e della Ricerca through the project SIR 2014 "THALMIGEN – Thallium: Mineralogy, Geochemistry, and Environmental Hazards", granted to CB. We are grateful to the staff of GAIA S.p.A., and in particular to Francesco Di Martino, for providing us with the pipeline samples used in this study and for useful information about the Valdicastello Carducci water treatment plant. We thank Massimo Onor of CNR-ICCOM, Pisa, for the information concerning Tl speciation in the Molini di Sant'Anna spring water, and Kirk G. Scheckel of United States Environmental Protection Agency, Washington, D.C., who kindly provided the standard spectrum for aqueous TlCl. The comments of five anonymous reviewers helped us improving the paper.

References

Agarwal, A., Vishnoi, A.N., 2005. XANES studies of thallium compounds and valence states and local environment of thallium in some of its superconducting cuprates. Phys. Scripta T115, 534-537.

Ankudinov, A.L., Ravel, B., Rehr, J.J., Conradson, S.D., 1998. Real-space multiple-scattering calculation and interpretation of x-ray-absorption near-edge structure. Phys. Rev. B 58, 7565-7576.

Anthony, J.W., Bideaux, R.A., Bladh, K.W., Nichols, M.C., 1990. Handbook of Mineralogy. Mineral Data Publishing, Tucson, Arizona, USA.

Biagioni, C., D'Orazio, M., Vezzoni, S., Dini, A., Orlandi, P., 2013. Mobilization of Tl-Hg-As-Sb-(Ag,Cu)-Pb sulfosalt melts during low-grade metamorphism in the Alpi Apuane (Tuscany, Italy). Geology 41, 747-750.

Brown, I.D., 2002. The chemical bond in inorganic chemistry: the bond valence model (Vol. 12). Oxford University Press on Demand.

Campanella, B., Onor, M., D'Ulivo, A., Giannecchini, R., D'Orazio, M., Petrini, R., Bramanti, E., 2016. Human exposure to thallium through tap water: A study from Valdicastello Carducci and Pietrasanta (northern Tuscany, Italy). Sci. Total Environ. 548-549, 33-42.

Calderoni, G., Giannetti, B., Masi, U., 1983. Abundance and behavior of thallium in the K-alkaline rocks from the Roccamonfina Volcano (Campania, southern Italy). Chem. Geol. 38, 239-253.

China MH, (Ministry of Health), 2006. Standard for drinking water quality (GB5749-2006).

d'Acapito, F., Trapananti, A. and Puri, A., 2016. LISA: the Italian CRG beamline for x-ray Absorption Spectroscopy at ESRF. J. Phys.: Conference Series 712, 012021.

D'Orazio, M., Biagioni, C., Dini, A., Vezzoni, S., 2017. Thallium-rich pyrite ores from the Apuan Alps, Tuscany, Italy: constraints for their origin and environmental concerns. Mineral. Dep., in press

Davies, M., Figueroa, L., Wildeman, T., Buckman, C., 2016. The oxidative precipitation of thallium at alkaline pH for treatment of mine influenced water. Mine Water Environ. 35, 77-85.

Dutrizac, J. E., Chen, T. T., Beauchemin, S., 2005. The behaviour of thallium (III) during jarosite precipitation. Hydrometallurgy 79, 138-153.

Giannecchini, R., 2006. Relationship between rainfall and shallow landslides in the southern Apuan Alps (Italy). Nat. Hazards Earth. Syst. Sci. 186, 357-364.

Hammond, C.R., 2004-2005. Properties of the elements and inorganic compounds. In: Lide D.R. (ed.). Handbook of chemistry and physics, 85th ed. Boca Raton, CRC, 4-37 - 4-168.

Holland, T.J.B., Redfern, S.A.T., 1997. Unit cell refinement from powder diffraction data: the use of regression diagnostics. Mineral. Mag. 61, 65-77.

Keith, L.H., Telliard, W.A., 1979. Priority pollutants-I. A perspective view. Environ. Sci. Technol. 13, 416-423.

Krebs, W., 1981. The geology of the Meggen ore deposit. In: Wolf, K.H. (ed.), Handbook of stratiform and stratabound ore deposits, vol. 9, Elsevier, Amsterdam, 509–549.

Lattanzi, P., Benvenuti, M., Costagliola, P., Tanelli, G., 1994. An overview on recent research on the metallogeny of Tuscany, with special reference to the Apuane Alps. Mem. Soc. Geol. Ital. 48, 613–625.

Lee, P. A., Citrin, P. H., Eisenberger, P. T., Kincaid, B. M., 1981. Extended x-ray absorption fine structure—its strengths and limitations as a structural tool. Rev. Modern Phys. 53, 769-806.

Léonard, A., Gerber, G.B., 1996. Mutagenicity, carcinogenicity and teratogenicity of thallium compounds. Mutat. Res. 387, 47–53.

Ludden, J., Albarède, F., Coleman, M., 2015. The impact of geochemistry. Elements 11, 239–240.

Orlandi, P., Biagioni, C., Bonaccorsi, E., Moëlo, Y., Paar, W.H., 2012. Lead-antimony sulfosalts from Tuscany (Italy). XII. Boscardinite, $TlPb_4(Sb_7As_2)_{\Sigma 9}S_{18}$, a new mineral species from the Monte Arsiccio mine: occurrence and crystal structure. Can. Min. 50, 235-251.

558 Otto, H.H., Baltrusch, R., Brandt, H.J., 1993. Further evidence for Tl^{3+} in Tl-based
559 superconductors from improved bond strength parameters involving new structural data of cubic
560 Tl_2O_3. Phys. C. Supercond. 215, 205-208.
561 Peacock, C.L., Moon, E.M., 2012. Oxidative scavenging of thallium by birnessite: explanation
562 for thallium enrichment and stable isotope fractionation in marine ferromanganese precipitates.
563 Geochim. Cosmochim. Acta 84, 297-313.
564 Peter, A.L.J, Viraraghavan T., 2005. Thallium: a review of public health and environmental
565 concerns. Environ. Int. 31, 439-501.
566 Radtke, A.S., 1985. Geology of the Carlin gold deposit, Nevada, USA. US Geol. Surv. Prof.
567 Pap. 1267, 241-246.
568 Ralph, L, Twiss, M.R., 2002. Comparative toxicity of thallium(I), thallium(III) and
569 cadmium(II) to the unicellular alga *Chlorella* isolated from Lake Erie. Bull. Environ. Contam.
570 Toxicol. 68, 261-268.
571 Ravel, B., 2001. ATOMS: crystallography for the X-ray absorption spectroscopist. J. Synchr.
572 Rad. 8, 314–316.
573 Ravel, B., Newville, M., A.T.H.E.N.A., 2005. ATHENA, ARTEMIS, HEPHAESTUS: data
574 analysis for X-ray absorption spectroscopy using IFEFFIT. J. Synchr. Rad. 12, 537-541.
575 Sabrowsky, H., 1971. Zur Darstellung und Kristallstruktur von Tl_2O. Z. Anorg. Allg. Chem.
576 381, 266-279.
577 Scheckel, K.G., Lombi, E., Rock, S.A., McLaughlin, M.J., 2004. In vivo synchrotron study of
578 thallium speciation and compartmentation in Iberis intermedia. Environ. Sci. Technol. 38, 5095–
579 5100.
580 UDH, 2014. Traverse Mountain: thallium in drinking water, Lehi, Utah County, Utah. Utah
581 Department of Health, Healt Consultation, Public Comment Version, 80 pp.
582 Vanysek, P., 2004. Electrochemical series. In: Lide DR Editor-in-Chief. Handbook of
583 chemistry and physics, 85th ed. Boca Raton: CRC; 2004-2005. p. 8-23 - 8-33.

584 Volkov, A.V., Serafimovski, T., Kochneva, N.T., Tomson, I.N., Tasev, G., 2006. The Alshar
585 epithermal Au-As-Sb-Tl deposit, southern Macedonia. Geol. Ore Dep. 48, 175-192.
586 Wedepohl, K.H., 1995. The composition of the continental crust. Geochim. Cosmochim. Acta
587 59, 1217-1239.
588 WHO, 2008. Guidelines for Drinking-water Quality. Volume 1, Recommendations (third
589 edition incorporating the first and second addenda ed.). World Health Organition, 2008, 515 p.
590 Xiao, T.F., Guha, J., Liu, C.Q., Zheng, B.S., Wilson, G., Ning, Z.P., He, L.B., 2000. Potential
591 health risk in areas of high natural concentrations of thallium and importance of urine screening.
592 Appl. Geochem. 22, 919–929.
593 Xiao, T.F., Guha, J., Boyle, D., Liu, C.-Q., Zheng, B., Wilson, G.C., Rouleau, A., Chen, J.,
594 2004. Naturally occurring thallium: a hidden geoenvironmental health hazard? Environ. Intern. 30,
595 501–507.
596 Xiong, Y., 2009. The aqueous geochemistry of thallium: speciation and solubility of thallium in
597 low temperature systems. Environ. Chem. 6, 441–451.
598 Zhang, Z., Chen, G., Zhang, B., Chen, Y., Zhang, X., 2000. The Lanmuchang Tl deposit and its
599 environmental geochemistry. Science in China 43, 50–62.
600

Table Captions

Table 1. Selected physico-chemical features of the water from the Molini di Sant'Anna spring during the period October 2014 - April 2016.

Table 2. ICP-MS analyses (μg/g) of rust scales lining the internal surface of the pipeline. The standard deviations of three repeated analyses are given within parentheses.

Table 3. Results of the leaching experiments on Tl-rich rust scales.

Table 4. Multiparameter fit details. CN is the coordination number, R is the path lenght, and σ is the Debye-Waller factor. The errors as calculated by ARTEMIS are indicated in parentheses.

Figure Captions

Fig. 1. Sketch map of the study area. Circled numbers refer to the aqueduct pipeline samples investigated in this study.

Fig. 2. Images of the rust scales lining the internal surface of the aqueduct pipeline samples studied in this work. (a) Pipeline sample P#2 cut in half longitudinally; (b) optical stereomicroscope images of rust scales of sample P#1; (c) back-scattered electron image of a small fragment of sample P#1 showing a homogeneous reflectivity; (d) back-scattered electron image of a small fragment of sample P#2 showing highly reflective spots peppering the surface.

Fig. 3. Back-scattered electron images of rust scales showing details of the highly reflective, Tl-rich phases. (a) Micrometer-sized spherules of Tl_2O_3 (light grey) on Fe-hydroxides (dark grey); (b) micrometer-sized spherules of Tl_2O_3 (light grey) showing their onion-shell internal structure; (c) enlarged view of the upper right area of (b); (d) encrustation of TlCl (light grey) on Fe-hydroxides (dark grey); (e) enlarged view of (d) showing partially dissolved TlCl crystals; (f) Tl_2O_3 microspherule (light grey, upper center) close to a tiny TlCl encrustation (light grey, lower center).

Fig. 4. X-ray powder diffraction pattern of Tl_2O_3 micro-spherules taken from sample P#3 (upper black line) and Tl_2O_3reflections calculated from the structural model of Otto et al. (1993) (lower grey lines). The *d* values (in Å) and *hkl* indexes are shown for each reflection.

Fig. 5. XRF spectra collected in situ on the rust scales of samples P#1 and P#2.

Fig. 6. Back-scattered electron images of cubic microcrystals of TlCl.

Fig. 7. Pictures of a test tube taken at increasing times and showing the progressive precipitation of Tl_2O_3 (dark brown) from a high-Tl solution after the addition of diluted NaOCl. See text for details.

630 **Fig. 8.** Normalized (a) and first derivative (b) Tl L_3-edge XANES for measured samples and
631 standards. TlCl (*aq.*) spectrum after Scheckel et al. (2004). In (a), main edge crests are found at
632 ~12681 and ~12687 eV for Tl(I) and Tl(III) compounds, respectively. In (b), the peaks in the
633 derivatives indicate the position of the main inflection point, which, by convention, is considered to
634 be the absorption edge energy. It can be seen that all Tl(I) standard compounds have an absorption
635 edge at ~12665 eV, while Tl_2O_3 at ~12669 eV. In (c) and (d), Tl L_3-edge EXAFS and Fourier
636 transform of measured samples are shown, respectively. Black lines are data, red lines are fits.

637

638 **Table 1**

639 Selected physico-chemical features of the water from the Molini di Sant'Anna spring during the
640 period October 2014 - April 2016.

Hydrochemical facies	calcium bicarbonate
*p*H	7.0 - 7.5
Average flow	40 L s^{-1}
(min-max)	(10 - 200)
Average Tl content	15 µg L^{-1}
(min-max)	(4 – 37)
Electrical conductivity (20°C)	315 – 575 µS cm^{-1}

641

642 **Table 2**

643 ICP-MS analyses (wt%) of rust scales lining the internal surface of the pipeline. The in-run errors (1
644 x SD of 3 replicate analyses) on the last digit are indicated in parentheses. "-" = not determined.

Sample	P#1	P#2	P#3
Tl	0.0092(1)	5.3(2)	1.52(1)
Al	0.14 (1)	0.16(2)	0.12 (1)
Mn	0.434(3)	0.41(1)	0.31(4)
Zn	0.0760(9)	-	-

645

Table 3

Results of the leaching experiments on Tl-rich rust scales. The in-run errors (1 x SD of 3 replicate analyses) on the last digit are indicated in parentheses.

Sample weight (mg)	Available Tl (mg)	Tap water added (mL)	Filtration (µm)	Tl conc. in the leachate (mg L^{-1})	% of solubilized Tl
97.30	1.48	20	none*	17.7(2)	24
97.30	1.48	20	0.20	17.7(1)	24
97.30	1.48	20	0.45	17.4(2)	24
97.30	1.48	20	none	18.2(2)	25
104.48	1.59	20	0.20	16.66(3)	21
104.48	1.59	20	0.45	16.1(2)	20
53.01	0.81	50	0.20	4.59(3)	29
23.36	0.36	50	0.20	1.85(1)	26
149.98	2.28	10	0.20	42.5(2)	19

*Sample centrifugated at 11000 rpm for 5 min.

652 **Table 4**

653 Multiparameter fit details. CN is the coordination number, R is the path lenght, and σ is the Debye-
654 Waller factor. The errors as calculated by ARTEMIS are indicated in parentheses.

	Path	CN	R(Å)	σ^2 (Å^2)
Tl_2O_3				
	Tl–O	5.8(2)	2.24(1)	0.007(1)
	Tl–Tl	2.6(6)	3.51(1)	0.007(2)
	Tl–Tl	5(1)	3.52(1)	//
P#2				
	Tl–O	5.2(2)	2.21(1)	0.014(2)
	Tl–Tl	1.4(7)	3.49(2)	0.011(5)
	Tl–Tl	2(1)	3.51(2)	//
res_P#2				
	Tl–O	5.2(2)	2.20(1)	.014(1)
	Tl–Tl	1.2(4)	3.47(1)	.007(3)
	Tl–Tl	2.4(8)	3.49(1)	//
P#3				
	Tl–O	1.7(4)	2.20(2)	0.008(3)
	Tl–Tl	0.8(5)	3.49(4)	0.015(9)
	Tl–Tl	2(1)	3.51(4)	//

655

656

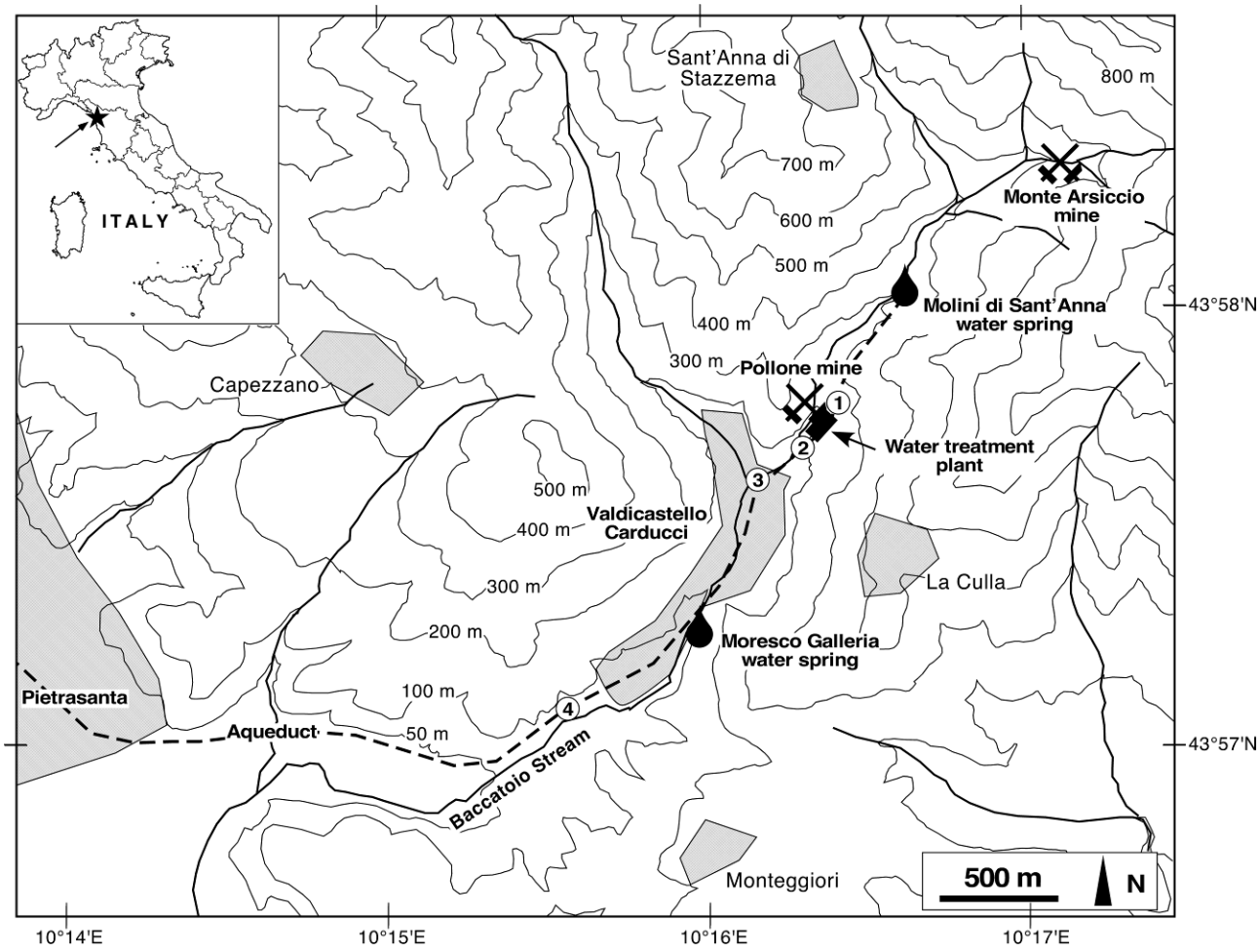

Fig. 1. Sketch map of the study area. Circled numbers refer to the aqueduct pipeline samples investigated in this study.

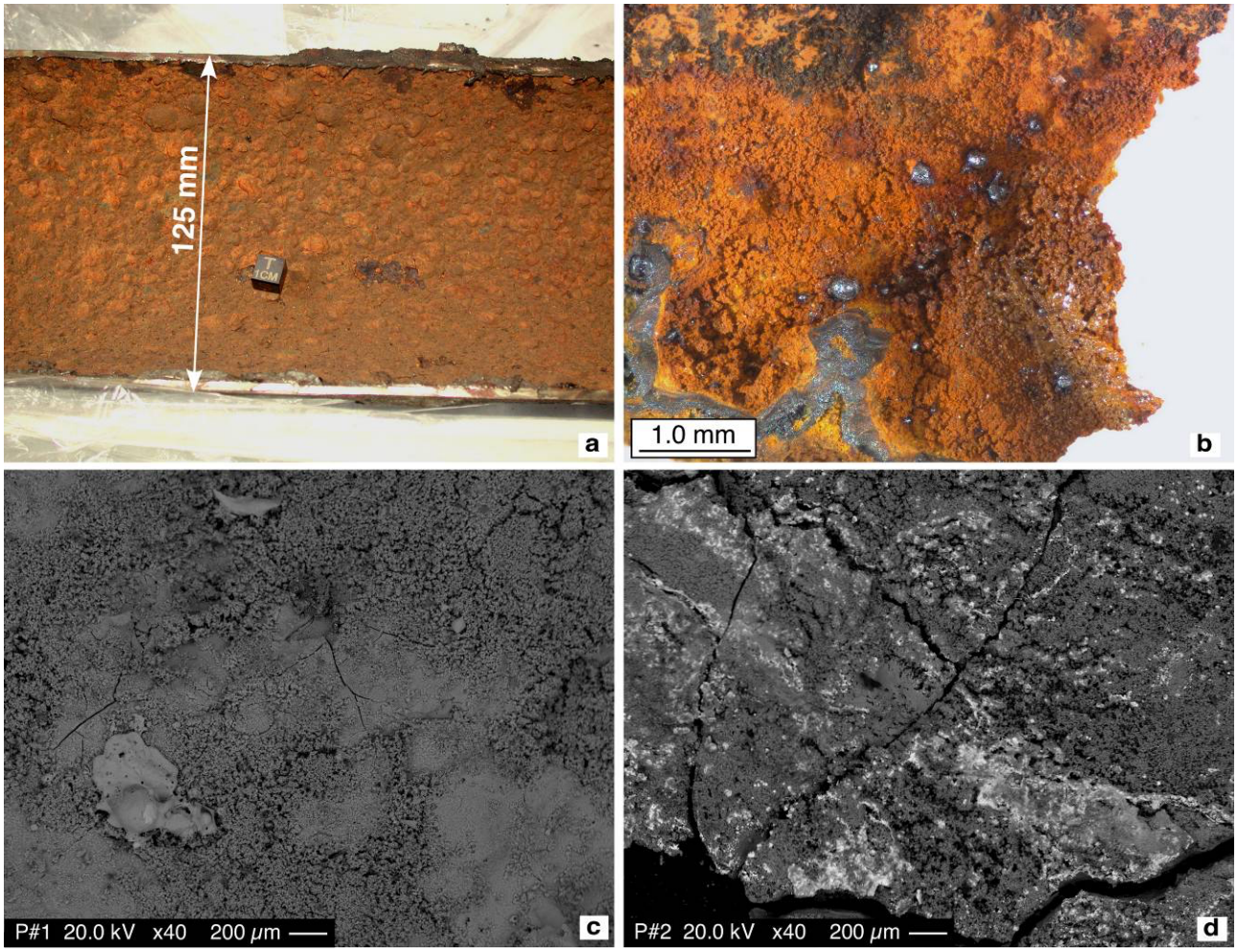

Fig. 2. Images of the rust scales lining the internal surface of the aqueduct pipeline samples studied in this work. (a) Pipeline sample P#2 cut in half longitudinally; (b) optical stereomicroscope images of rust scales of sample P#1; (c) back-scattered electron image of a small fragment of sample P#1 showing a homogeneous reflectivity; (d) back-scattered electron image of a small fragment of sample P#2 showing highly reflective spots peppering the surface.

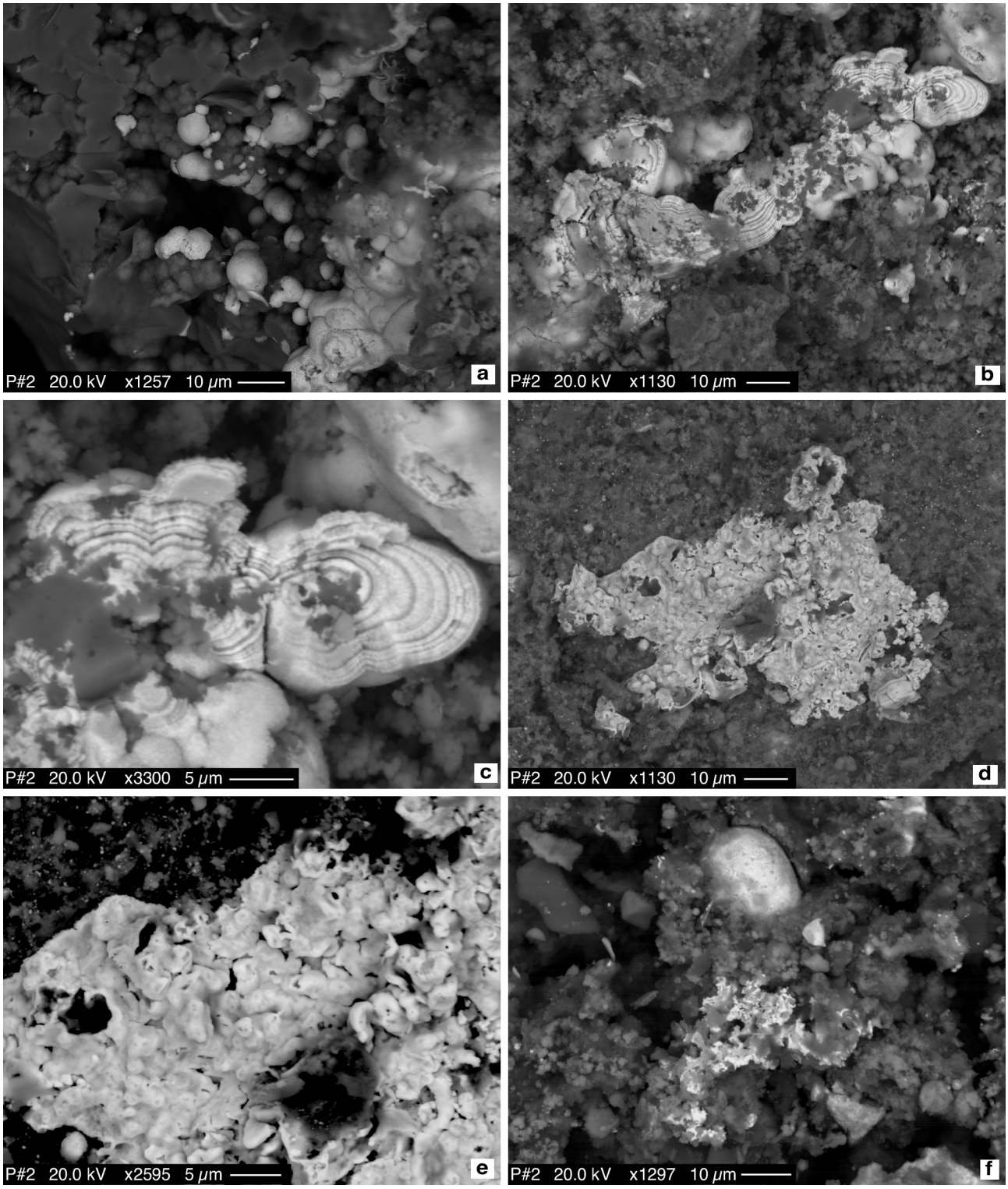

667

668 **Fig. 3**. Back-scattered electron images of rust scales showing details of the highly reflective, Tl-rich
669 phases. (a) Micrometer-sized spherules of Tl_2O_3 (light grey) on Fe-hydroxides (dark grey); (b)
670 micrometer-sized spherules of Tl_2O_3 (light grey) showing their onion-shell internal structure; (c)
671 enlarged view of the upper right area of (b); (d) encrustation of TlCl (light grey) on Fe-hydroxides
672 (dark grey); (e) enlarged view of (d) showing partially dissolved TlCl crystals; (f) Tl_2O_3
673 microspherule (light grey, upper center) close to a tiny TlCl encrustation (light grey, lower center).

674

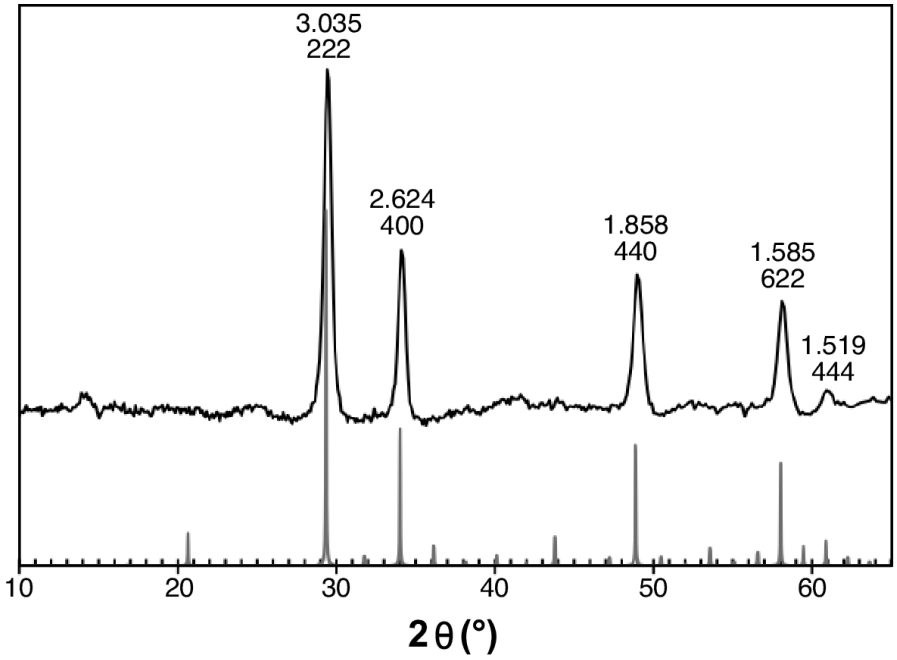

675

676 **Fig. 4**. X-ray powder diffraction pattern of Tl_2O_3 micro-spherules taken from sample P#3 (upper
677 black line) and Tl_2O_3reflections calculated from the structural model of Otto et al. (1993) (lower
678 grey lines). The *d* values (in Å) and *hkl* indexes are shown for each reflection.

679

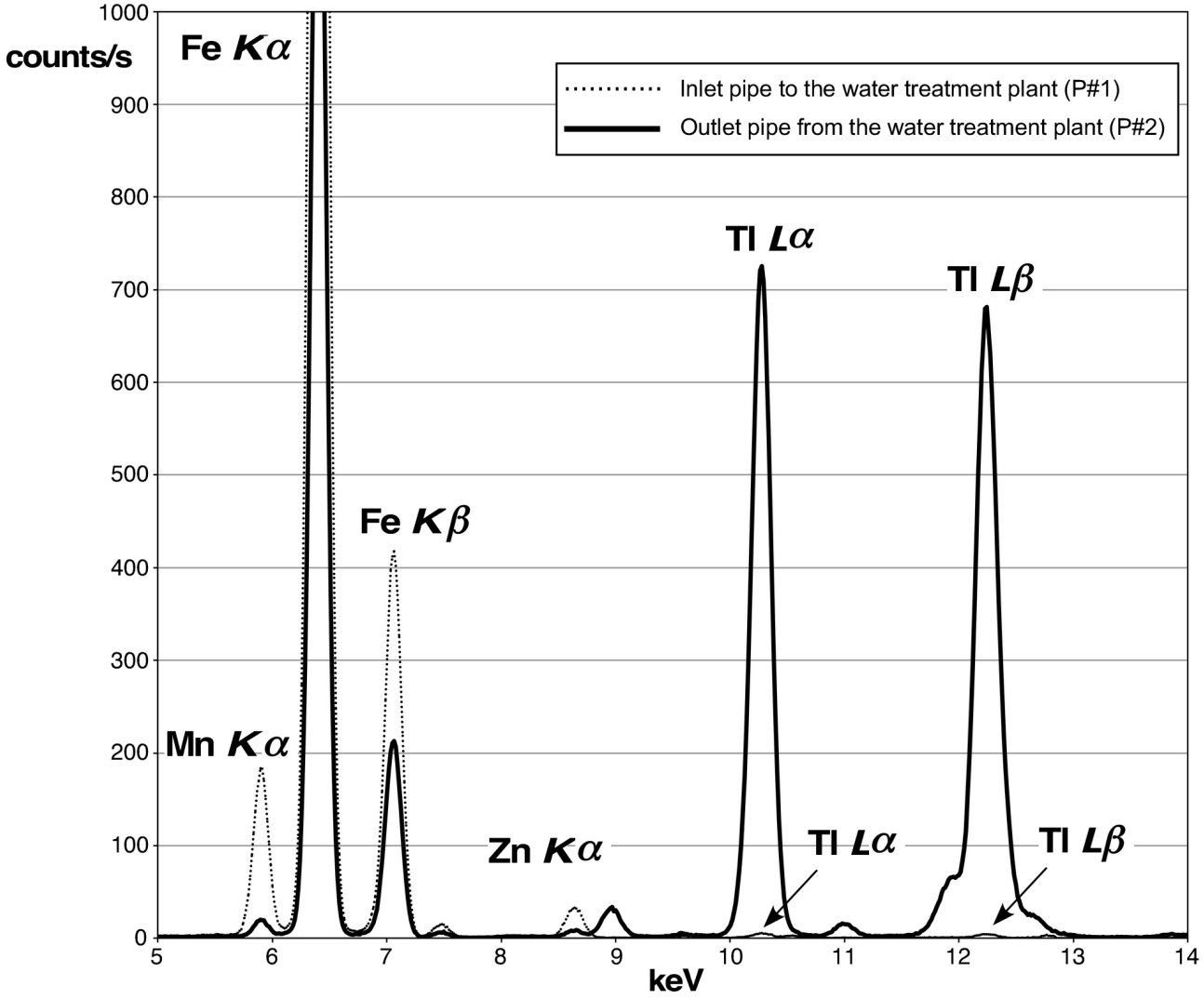

680

681 **Fig. 5**. XRF spectra collected in situ on the rust scales of samples P#1 and P#2.

682

683 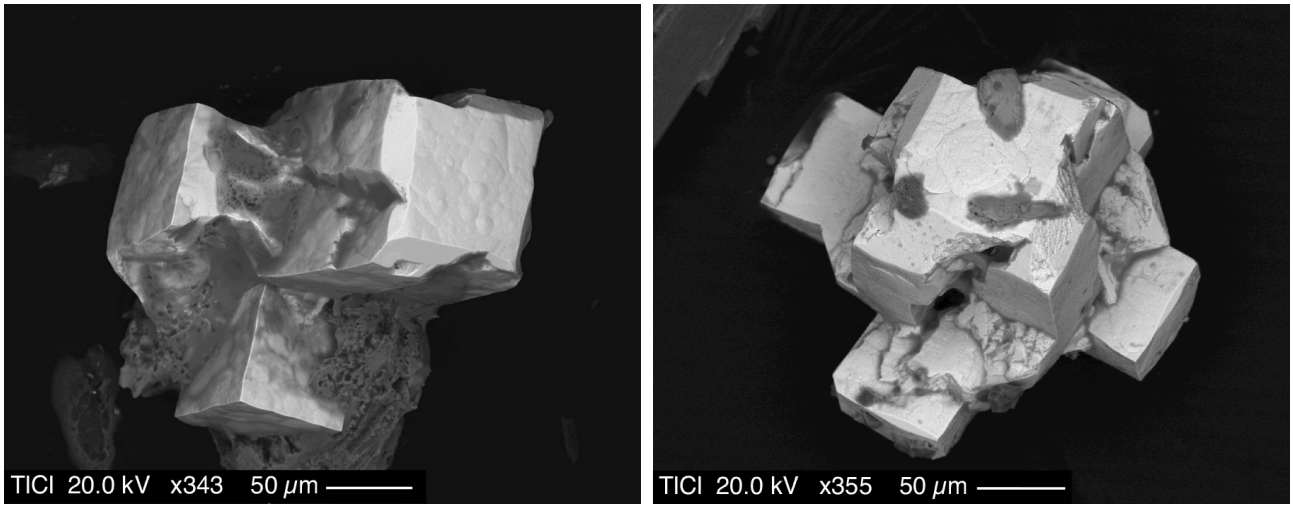

684 **Fig. 6**. Back-scattered electron images of cubic microcrystals of TlCl.

685

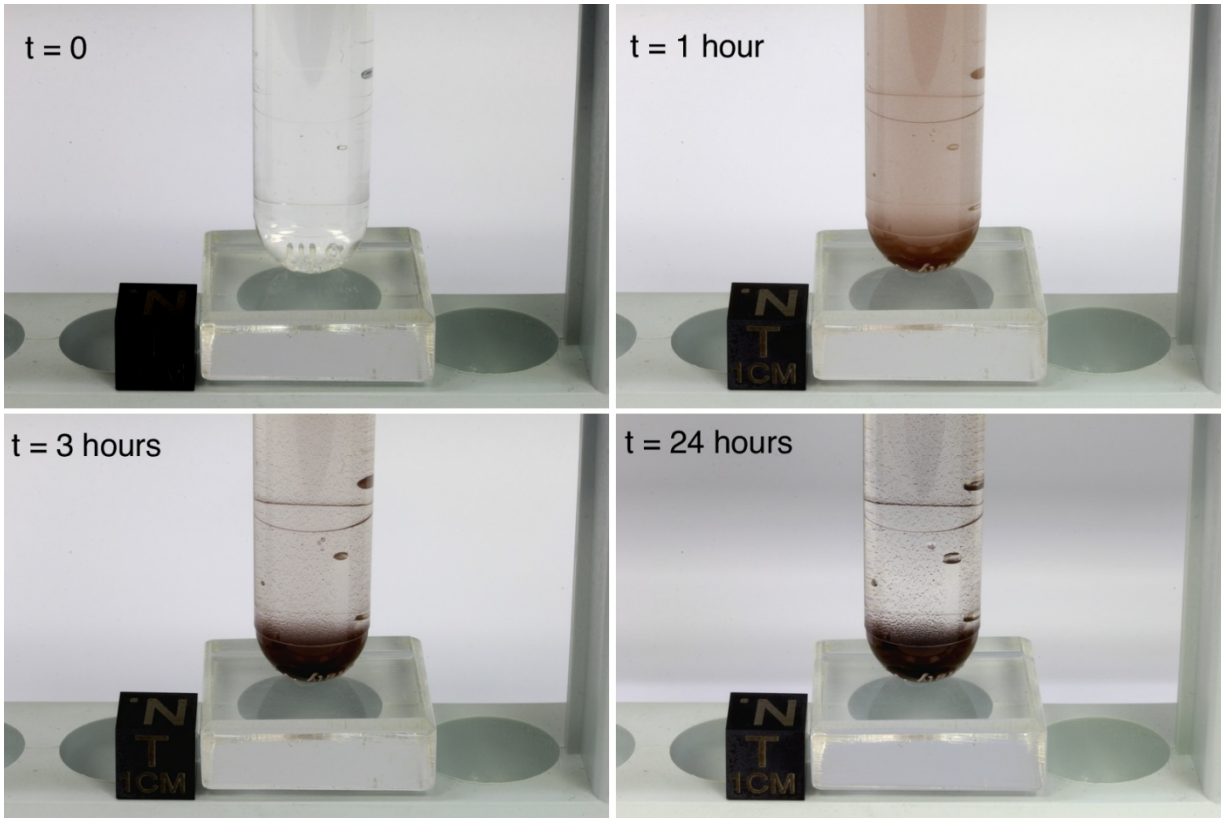

686

687 **Fig. 7**. Pictures of a test tube taken at increasing times and showing the progressive precipitation of
688 Tl_2O_3 (dark brown) from a high-Tl solution after the addition of diluted NaOCl. See text for details.

689

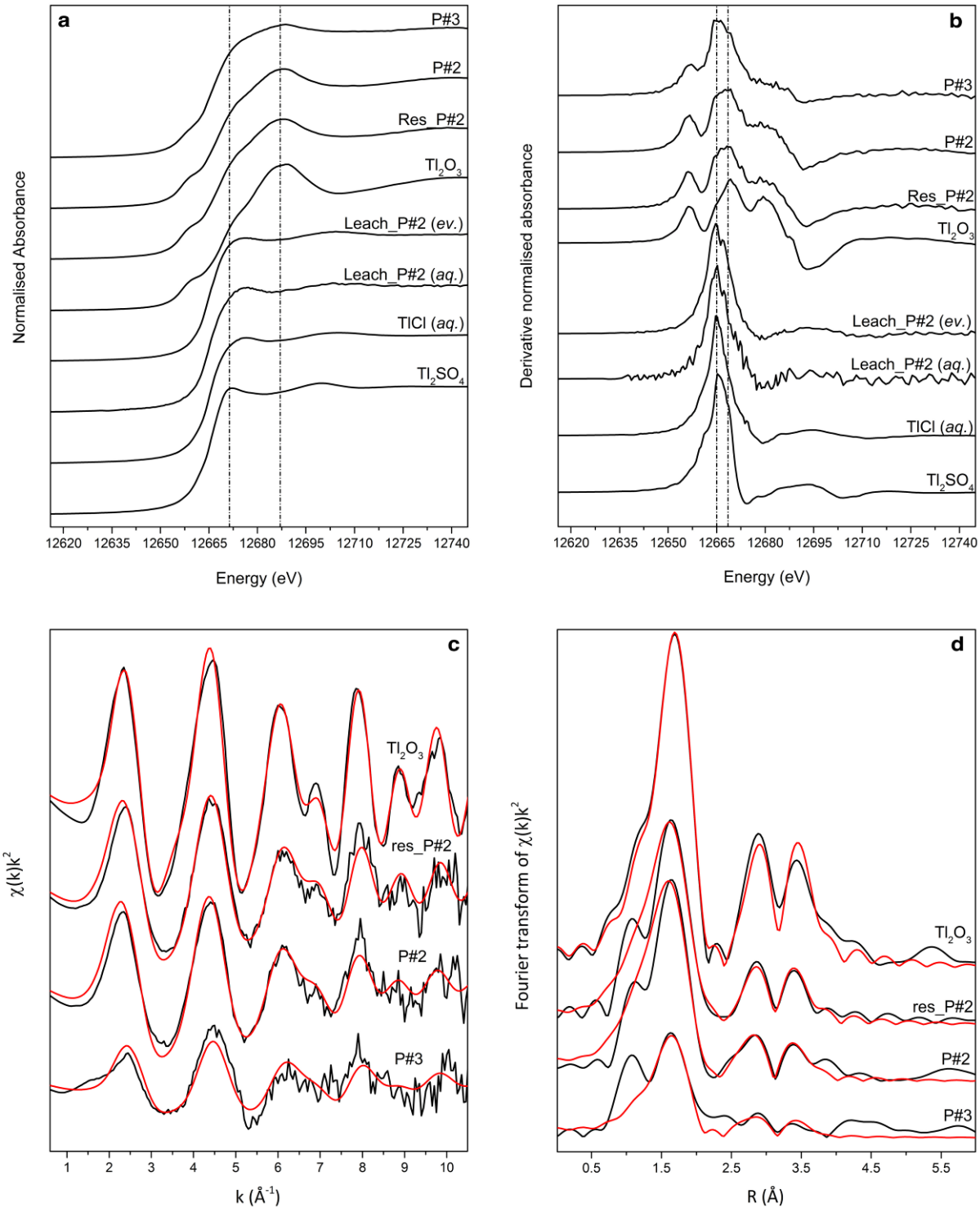

690

691 **Fig. 8.** Normalized (a) and first derivative (b) Tl L_3-edge XANES for measured samples and
692 standards. TlCl (*aq.*) spectrum after Scheckel et al. (2004). In (a), main edge crests are found at
693 ~12681 and ~12687 eV for Tl(I) and Tl(III) compounds, respectively. In (b), the peaks in the
694 derivatives indicate the position of the main inflection point, which, by convention, is considered to
695 be the absorption edge energy. It can be seen that all Tl(I) standard compounds have an absorption
696 edge at ~12665 eV, while Tl_2O_3 at ~12669 eV. In (c) and (d), Tl L_3-edge EXAFS and Fourier
697 transform of measured samples are shown, respectively. Black lines are data, red lines are fits.